Neutron-evaporation analysis of ^{44}Ca-induced reactions on trans-lanthanide targets.

A thesis submitted in partial fulfilment of the requirements for the award of degree of

Master of Science

In

Physics

Submitted by

Trisha Walia

(Roll No.:- 301404029)

Under the supervision of

Dr. Manoj K. Sharma

(Head and Professor of Physics)

SPMS

Thapar University, Patiala

School of Physics and Materials Science (SPMS)

Thapar University,

(Formerly Thapar Institute of Engineering and Technology)

Patiala-147004, INDIA

June- 2016

A grateful heart is a beginning of greatness

I dedicate this thesis to my parents *RAKESH MOHAN WALIA* and *NEELAM WALIA* . I am really thankful for providing me the best education and inspiring me so that i can accomplish my dreams.

CERTIFICATE

I hereby certify that the work which has been presented in this thesis entitled, "**Neutron-evaporation analysis for ^{48}Ca-induced reactions on trans-lanthanide nuclei**" submitted in partial fulfilment of the requirements for the award of degree of **Master of Science** in **Physics** at **Thapar University, Patiala**, is an authentic record of my own work carried out under the supervision of Mr. **Manoj K. Sharma, Head and Professor of SPMS** and refers other researcher's work which are duly listed in reference section.

The matter embodied in this thesis has not been submitted for the award of any other degree of this or any other university.

Date: 15/7/2016

(TrishaWalia)

This is to certify that the above statement made by the candidate is correct and true to best of my knowledge.

Dr. Manoj K. Sharma
(Head and Professor of Physics)
SPMS
Thapar University,
Patiala

Counter signed by

Dr. Manoj K. Sharma
(Head and Professor of Physics)
SPMS
Thapar University,
Patiala-147001

Dr. S.S. Bhatia,
Dean of Academic affairs
Thapar University,
Patiala, 147001

ACKNOWLEDGMENT

Thanks to the merciful lord for all the countless blessings you have offered me, and thanks to my parents for their love and support.

It is a great pleasure to acknowledge my deepest thanks and gratitude to **Prof. Manoj K. Sharma, Head and Professor, SPMS,** for suggesting the topic of this dissertation, and his kind supervision. It is a great pleasure to work under his supervision.

It is genuine pleasure to express my deep sense of thanks and gratitude to my mentor, philosopher, guide and friend **Amandeep Kaur Jagdeo.** Her dedication and keen interest and above all her overwhelming attitude to help me had been solely responsible for completing my work. Her prompt inspirations, timely suggestions with kindness, enthusiasm, dynamism scholarly advice and scientific approach have enabled me to complete my thesis.

I also want to thank my friends Amandeep Kaur Jagdeo, Amandeep Caur, Amantej Kaur Lotay, Monika Gorsi, Kaifi Sehgal, Arunima Sanghi, Allaiyah Walia for their support and with whom I created unforgettable memories during my thesis work. I also want to thank my family, who taught me the value of hard work by setting their own example

Date: 15/7/2016

Trisha Walia

Abstract

Dynamical cluster decay model (DCM) has been applied to study the dynamics of ^{44}Ca induced reactions. The DCM based neutron based ^{44}Ca-induced reactions on trans-lanthanide targets agree nicely with experimental data. The following reactions are studied and worked upon over a wide range of incident energies.

- $^{44}Ca+^{158}Gd \rightarrow ^{202}Po^{*} \rightarrow ^{199}Po+3n$
- $^{44}Ca+^{159}Tb \rightarrow ^{203}At^{*} \rightarrow ^{200}At+3n$
- $^{44}Ca+^{162}Dy \rightarrow ^{206}Rn^{*} \rightarrow ^{203}Rn+3n$

This dissertation comprises of three chapters.

Chapter-1:

Chapter-1 consists of the basic over-view of nuclear reactions, compound nucleus formation, neutron evaporation and deformations and orientations.

Chapter-2:

Chapter-2 consists of the description of dynamical cluster decay model (DCM). It gives description about the various potentials used in DCM, mass-dependent level density parameter along with other parameters of the model. The deformation effects of decaying fragments are included in the framework of DCM.

Chapter-3:

Chapter-3 consists of the details of the DCM based calculations for the above mentioned reactions and the fragmentation behaviour of the chosen reactions is analysed in view of pre-formation factor and barrier penetrability.

Contents

Chapter-3

Results and discussions…….....33

List of figures:

Chapter-1

Chapter-2

Chapter-3

Fig 3.8 DCM based cross-sections and experimental data for composite systems $^{202}Po^{*}$, $^{203}At^{*}$ and $^{206}Rn^{*}$.

List of tables:

Chapter-3

CHAPTER 1

Literature survey

1.1 Introduction

Since ages human brain has tendency to explore new things as they unfold to him, which has lead to various discoveries and inventions and this curiosity has always been the driven force to explore every bit of the universe. The endless efforts and worthy endeavours by human minds lead to the discovery of electron which shattered the age long myth of the atom to be the building block of all material objects. In 1897, J.J. Thomson proposed the plum pudding model of the atom in which there was the sea of positive charge in which the electrons were embedded like raisons in plum pudding. This model acted like the stepping stone which made us to have an insight of the atom. But Henry Becquerel while working with uranium salts, observed the spontaneous emission of certain sub-atomic particles which accelerated the investigations regarding atomic dissipation. And eventually the Rutherford α-ray scattering experiment gave the clear picture about the existence of the ***'nucleus'*** as the centre of the atom where whole of the mass and positive charge of the atom was supposed to be concentrated. This leads the scientists further towards a new branch of physics called the *'nuclear physics'* which deals with the investigation of the core of the atom known as 'nucleus'.

This arose many questions regarding composition of the nucleus and various theories were put forward which included the coexistence of protons and electrons within the nucleus so as to retain the electrical neutrality and to overcome Columbic repulsions between the protons. But this theory was discarded due to certain drawbacks. The discovery of neutron in 1932 led to the proton-neutron theory, according to which the proton along with its neutral counterpart neutron exists inside the nucleus-the core of every atom. Despite of the electrostatic repulsions, the co-existence of positively charged protons inside the small region of nucleus suggested that some extremely strong force exist inside the nucleus known as 'nuclear force'.

The nucleus is considered to be a unique ensemble of large but finite number of interacting nucleons. Both single particle (out of phase) and collective (in phase) effects occur inside a nucleus. As nucleus is a many body problem of great complexity, hence a physical insight into its wide range of properties is needed, which is given by nuclear models. The usefulness of a model is tested by its ability to provide predictions that can be verified experimentally. Nuclear models are classified into two groups, out of which the first group corresponds to independent particle models having no interaction between the individual particles, the

Shell model description. The other group corresponds to statistical models, in which protons and neutrons are assumed to be mutually coupled to each other.

The Liquid Drop Model was the first model to describe the nuclear behaviour, in which a nucleus was considered analogous to a drop of liquid, was based on the assumption that nucleus has energy which is due to surface tension and electrostatic repulsion of protons and also that forces acting on nucleons at the surface of a nucleus are different from the forces acting on the nucleons inside it. The LDM helped in giving a good idea regarding nuclear fission and fusion as it was able to account for variation of the binding energy per nucleon as a function of mass number. Its main drawback was that, it could not explain the magic number (the stable nuclei having specific number of protons and neutrons).

To resolve this issue, a new model based on microscopic approach of Pauli's exclusion principle, called shell model was introduced. With the help of spin orbit interaction, it was able to explain the nuclear structure in terms of energy levels and shells which further helped in explaining the magic numbers and addressing magnetic moments. The Collective Model (developed by Aage Bohr and Ben Mottleson), exhibit extension of these models by including motions of the whole nucleus such in terms of rotational and vibration degree of freedom. The Collective Model emphasizes the coherent behaviour of all of the nucleons. Hence, the two extremes of the behaviour nucleons in the nucleus are represented by the shell model and collective model. The combination of both shell and collective model leads to more realistic approach known as unified model.

The investigation regarding the nuclear structure is done with the help of nuclear reactions in which a projectile nucleus having certain energy is made to hit on the target nucleus. Depending upon the energy of the projectile, the nuclear reactions can be characterized as low, intermediate and high energy reactions. The different energy ranges are: (i) **Low energy**: The energy of reactions is less than 15 MeV/nucleon and in this range we study nuclear shapes, size, basic properties, resonance, models, reactions, dynamics, super heavy symmetries, halo shapes, fusion-fission, particle evaporation, quasi-fission, incomplete fusion etc. (ii) **Intermediate energy**: The energy of reactions is in between 15-500 MeV/nucleon and in this range we study multi fragmentation, particle production, nuclear flow, balance energy etc. (iii) **High energy**: The energy of the reaction is greater than 500MeV/nucleon and it gives qualitative detail about neutrons, protons, quarks, mesons and other elementary particles.

It is relevant to mention here that the present work is confined to low energy nuclear reactions only.

1.2 Nuclear reactions

A nuclear reaction refers to a process in which a nucleon or a nucleus comes closer to the target nucleus by overcoming the Columbic barrier (that exists between the protons) and transmitting their energy to the nucleons of target nucleus. Subsequently the energy and momentum exchange takes place to form new nuclear particles which intern help in understanding the nuclear structures, and thus provide information about various nuclear phenomena. The major players of a nuclear reaction are the *nucleons*. Earlier, the common projectiles used were alpha particles, beta particles and gamma rays, obtained from the process of radioactivity, and eventually the heavy ion beams were produced and used for the purpose.

The low energy beams of neutrons can easily penetrate the Columbic barrier and is a very common source generally used in nuclear power plants. With the advancement in technology and the advent of particle accelerators, it is not only possible to produce high energy beams of protons, neutrons or α-particles, but also of heavy ions (heavier than α-particle) and thus led to various new types of nuclear reactions**.** Nuclear reactions involving projectiles which have $Z \geq 2$ and $A \geq 4$ are known as heavy ion reactions and corresponding projectiles are termed as heavy ion beams. Also certain radioactive ion beams along with heavy ion beams have been used to produce elements lying in heavy and super-heavy region, and has took the branch of nuclear physics to new horizons. These reactions help in further investigation of nuclear phenomena and associated nuclear forces. Amongst various applications of nuclear reactions, the production of exotic nuclear systems near and beyond drip line and the synthesis of new heavy/super-heavy elements have been at the driving seat during last few decades. The heavy ion induced reactions generally commence via compound nucleus path and a brief description of the same is discussed in the next section.

1.2.1 Compound nucleus formation and decay

The primary evidences on which the compound nucleus idea was developed came after the discovery of the neutron and its use as a projectile in producing nuclear reactions. However, for very low energies, the cross-section is higher. When a nuclear projectile hits the target nucleus for a nuclear reaction to occur, an intermediate state is formed as a result of

absorption of incident particle by the target nuclei, which is known as *compound nucleus.* The incoming projectile quickly dissipates its energy as it enters into the nucleus and merges with the closely packed nucleons in it. As a result, the general random motion of all the nucleons in the nucleus is disturbed, each nucleon gaining some additional energy. But no single one of them will generally gain enough energy to enable it to come out of the nucleus, which is of order of few MeV. However, after a relatively long time when certain number of collisions has occurred, enough energy may be concentrated on one or a bunch of nucleons enabling them to escape from the nucleus.

The decay products of the compound nucleus have been experimentally observed over various combinations of projectile and target interacted over a wide range of incident energy. Depending upon the mass of the compound nucleus and associated excitation level, it may decay via multiple paths, exhibiting variety of decay mechanisms. After a compound nucleus is formed, it forgets how it was formed and hence its decay generally don't depend upon its incident channel. The energy and momentum of the incident heavy ions [1] are shared among all the nucleons of the CN leading to the statistical equilibrium. The excited compound nucleus then decays to the final reaction product by emitting nuclear particles and/or gamma rays, and it is assumed that, mode of decay of the compound nucleus is independent of the mode of its formation.

The various modes in which compound nucleus can decay are:

1.2.1.1 Neutron evaporation: It is a process in which there is emission of 1, 2 or more number of neutrons, following the compound nucleus (CN) path. The nuclear reactions induced by heavy ions at moderate excitation energies give rise to a variety of processes. If energy of the incident ion is larger than the Coulomb barrier, it is absorbed by target nucleus forming a compound nucleus (CN). At moderate excitation energies, emission of charged particles from the compound nucleus is seriously hindered because of the Coulomb barrier. In such cases, the composite system formed by the amalgamation of the target nucleus with the incident ion de-excites via evaporation of many neutrons. The evaporation of neutrons may be considered as a random process. The compound nucleus releases a given fraction of its excitation energy which is independent of number of neutrons emitted in any other excitation energy interval. For excitation energies ranging between E_{CN}=10-20 MeV, the

possibility of 1n and 2n neutron evaporation is more, but as the excitation energy increases the 3n, 4n and 5n neutron evaporation becomes prominent[2].

1.2.1.2 Evaporation residue mode[3]: This decay mode forms a predominant channel for composite systems having mass range A=50-100, where fission is generally absent. The emitted fragments are generally the light particles like protons, deuterons, α-particles. In this case the compound nucleus formed is unstable and gets stabilised by emitting some energy in the form of protons, deuteron or α- particle. In this process the emitted fragments are $A_2 \leq 4$ and $Z_2 \leq 2$, where A_2 and Z_2 refer to the mass and charge of emitted fragment.

1.2.1.3 Fusion-fission mode: This decay mode is mostly found for composite systems having mass $A \geq 200$, due to its instability against Coulomb repulsion arising due to presence of large number of protons. The products formed during this mode are supposed to be symmetric i.e. they are of equivalent masses [4]. However, sometimes one may also find asymmetric fragments in the fission process. In case they become fairly asymmetric then the same are termed as heavy mass fragments (HMF).

1.2.2 Non-Compound nucleus decay mode(Quasi-fission):

The deep-inelastic collisions of heavy ion form very energetic nuclear reactions. Such reactions involve heavier ions and intermediate impact parameters and consequently proceed through non-compound nucleus channel. Within this reaction, if the emitted products are identical with the formation partners, the process is called quasi-fission (QF). In this process the projectile and target nuclei get re-separated before the formation of composite system (Compound nucleus) due to strong repulsive Columbic forces. The QF channel is generally applicable to higher incident energies and the fragments have different masses and angular momentums than for a fusion-fission channel [5]. It is expected that the incoming nuclei do not lose their identity during CN transition and as a result the decaying fragments remain identical to entrance channel [6-8]. Experiments have shown that tip to toe collisions result in quasi-fission and sideways collision result in fusion-fission. Quasi-fission is the major competing channel in super heavy region due to strong Coulomb repulsions. This process is orientation based i.e. if the actinide target (prolate deformed) is along the equatorial axis of the collision axis, the fusion-fission may happen at energies higher

than Coulomb barrier. On the other hand, if the colliding reaction partners are lying along the polar axis, then the QF channel starts competing with fusion-fission process.

1.3 Deformations and Orientations [9]

The shape of nucleus was first investigated by determination of electric quadrupole moment of the hyperfine structure of atomic spectra. The magic and near magic nuclei are generally spherical, but majority of nuclear systems arrange the protons and neutrons into deformed shells so as to lower their energy and become stable. These deformed shapes governs the electrical quadrupole moment

The quadrupole moment of evenly charged nuclei is given by:

$Q=2/5Z(b^2-a^2)$; where a and b are ellipsoid axes.

If Q=0, then nucleus is spherical in shape. For a>b, Q is –ve and we get an oblate spheroid. For a<b, Q is +ve and we get a prolate sphere

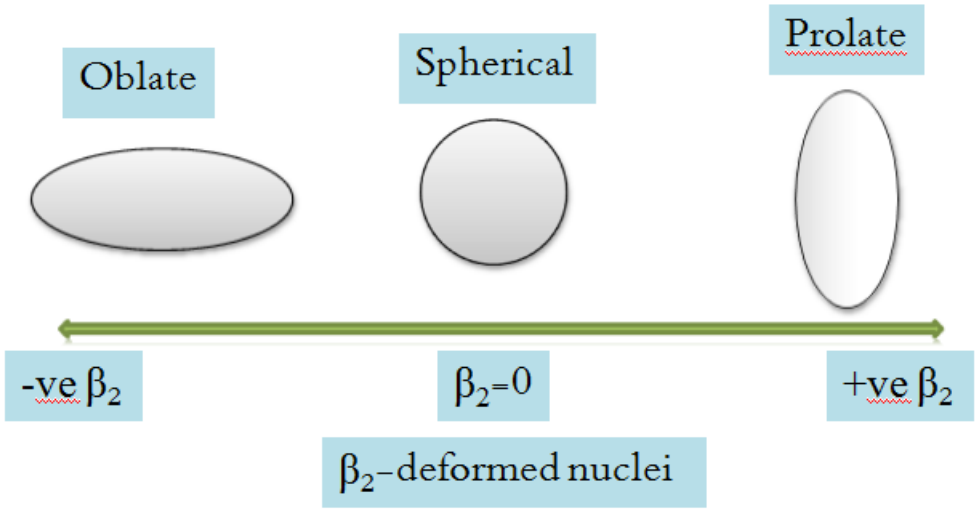

Fig 1.1 Quadrupole deformations

Here the most commonly observed deformed nuclear shapes are the prolate meaning elongated and oblate meaning flattened corresponding to λ=2 multipole, which describe the quad-oscillation of a nuclear surface. The λ=3 multipole represent octupole deformation which gives an idea about the octupole oscillations of a nuclear surface and hence gives

knowledge regarding reflection asymmetry in nuclear shape, which is a major reason behind pear like shape of nucleus.

In a nuclear reaction two nuclei are brought together to form a compound nucleus (CN). A substantial energy barrier, due to mutual repulsion between the two nuclei, opposes the fusion reaction. This barrier consists of the Coulomb and the nuclear potentials. However, the long range Coulomb repulsion between the nuclei is offset by stronger, but short range, attractive nuclear force. Then, the problem is to bring the nuclei sufficiently close so that the Coulomb barrier can be crossed over, say, via tunnelling. Hence, the two nuclei are required to collide with sufficient kinetic energy to overcome their mutual electrostatic repulsion and subsequently to bring into effect the role of strong but short range attractive nuclear force. The interaction potential and the fusion cross-sections are largely influenced by the nuclear structure effects of the target and projectile nuclei and their relative orientations. The collisions between the deformed as well as oriented fragment have been studied theoretically and experimentally to establish the effects of deformation and orientation on reactions.

A hot fusion reaction is characterized by the highest reaction barrier and smallest interaction radius and cold or compact reactions are characterized by the lowest reaction barrier and largest interaction radius i.e. for their 90^o, 90^o orientations, or equator cross-configuration. If one of a nuclei in a reaction is spherical and the other one deformed having a 90^o orientation, than the configuration is known as 'equatorial compact'. The importance of magnitude of both the quadropole (β_2) and hexadecouple (β_4) deformations of reaction partners in distribution of barriers in orientation degree of freedom is recently shown with the help of an article, based on generalized fragmentation theory, in which the orientation degree of freedom and higher multipole deformations are considered within the nuclear proximity potential [10]. If the nuclei involved has the quadruple deformations and a little addition of hexadecouple deformations and the other reaction partner is spherical, the specified configuration is belly to belly compact configuration. But the presence of large compact configuration does not lead to similar configuration. For compact configuration, however, the magnitudes of other higher multipole deformations play much more importance for distribution of barriers in orientation degrees of freedom, i.e., for the angle(s) of orientation. The sign of β_3 deformation is generally negative and it always favours equatorial compact configuration. The β_2, β_3 and β_4 are the main deformations considered, whereas β_6 deformations support the lower-order

deforamations. However for deformed-deformed collision, the role of β_6 is simply to support the result of β_4 or $\beta_3 + \beta_4$ and does not depends upon its sign.

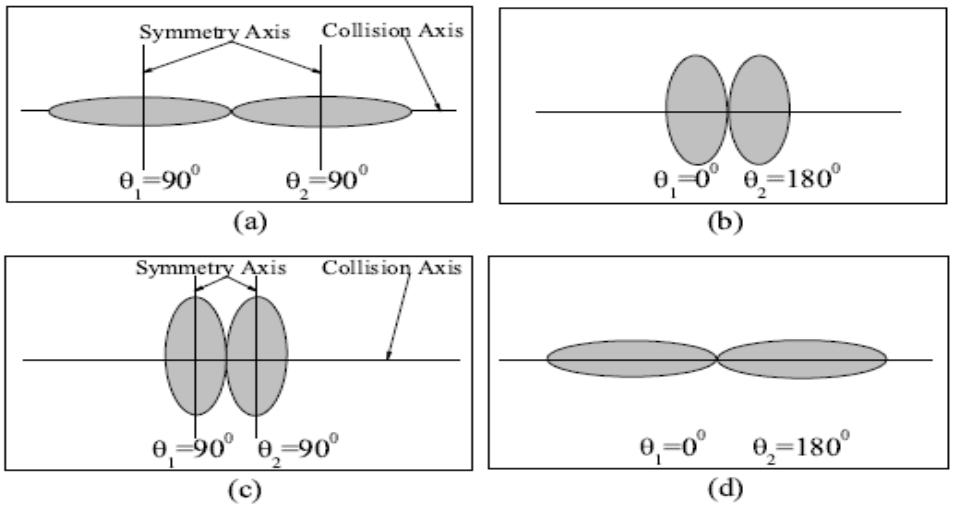

Fig 1.2 Schematic diagrams for deformed nuclei ((a),(b) oblate and (c),(d) prolate only) with corresponding optimum orientations along collision axis for" cold, elongated " ((a),(d)) or" hot, compact"((b),(c)) configuration[11].

A detailed study based upon Quantum Mechanical Fragmentation Theory (QMFT) [12-14] shows that the interaction barrier (height as well as its position) is greatly affected by deformed and oriented colliding nuclei. This study gives the optimum orientations for fusion of deformed nuclei based on the quadrupole deformations alone and also investigated the role of hexadecupole deformation in fusion reactions. The optimum orientations are given for cold, non-compact" and hot, compact" fusion configurations corresponding to largest interaction radius/lowest barrier and smallest interaction radius/highest barrier respectively [15-17]. However a schematic diagram is illustrated in Fig 1.2 only for prolate-prolate and oblate-oblate deformed colliding nuclei along collision axis for both "cold, elongated" and "hot, compact" configurations [11].

Motivation of present work

In the present work, the dynamics associated with decay of compound systems $^{202}Po^{*}$, $^{203}At^{*}$ and $^{206}Rn^{*}$ formed in ^{44}Ca induced reactions is explored within the framework of DCM [18]. The decay of compound systems $^{202}Po^{*}$, $^{203}At^{*}$ and $^{206}Rn^{*}$ is studied exclusively for neutron evaporation cross-sections i.e. 3n, 4n and 5n by optimizing neck-length parameter 'ΔR', which assimilates neck formation effort between decaying fragments. The calculations are done by including quadruple deformations (β_2) with optimum orientations for 'hot' configurations. The important point to note here is that, the role of mass-dependent level density parameter is analysed exclusively, and the usually taken constant values of level-density parameter are replaced with the mass-dependent expression as suggested in [19]. The DCM based cross-sections find nice agreement with experimental data. The decay patterns of the compound systems $^{202}Po^{*}$, $^{203}At^{*}$ and $^{206}Rn^{*}$ are investigated in form of the fragmentation and preformation curves and the effects of temperature and angular momentum on the potential energy surfaces are studied. In addition to this, the comparison of the fragmentation structures of all the three compound nuclear systems $^{202}Po^{*}$, $^{203}At^{*}$ and $^{206}Rn^{*}$ formed in ^{44}Ca induced reactions is made at common incident beam energy i.e. E_{beam}~ 189 MeV. The optimum values of neck length parameter ΔR and other ingredients of DCM are tabulated in Tables 3.1, 3.2 and 3.3

References

[1] Vijay R. Sharma *et al*., Phys. Rev. C 84, 014612 (2011).

[2] Anubhav Raghav,, Prabhat Kumar, Vijay R. Sharma, Abhishek Yadav, Devendra P. Singh, Pushpendra P. Singh, Manoj K. Sharma, Indu Bala, R. Kumar, B. P. Singh and R. Prasad. Proceedings of the DAE Symp. on Nucl. Phys. 58 (2013)

[3] M. Kumar, R. Kumar and M. K. Sharma, Phys. Rev. C 85, 014609 (2012)

[4] B. Ivle, Phys. Rev. C 87, 034619 (2013).

[5] J. Khuyagbaatar, K. Nishio, S. Hofmann, D. Ackermann, M. Block, S. Heinz, F. P. Hebberger, K. Hirose, H. Ikezoe, B. Kinlder, B. Lommel, H. Makii, S. Mitsuka, I. Nishinaka, T. Ohtsuki, Phys. Rev. C 86, 064602 (2012).

[6] D. J. Hinde, M. Dasgupta, J. R. Leigh, J. P. Lestone, J. C. Mein, C. R. Morton, J. O. Newton, and H. Timmers, Phys. Rev. Lett. 74, 1295 (1995).

[7] V. I. Zagrebaev, A. V. Karpov and Walter Greiner, Phys. Rev. C 81, 044608 (2010).

[8] E. Prasad, K. M. Varier, N. Madhavan, S. Nath, J. Gehlot, Sunil Kalkal, Jhilam Sadhukhan, G. Mohanto, P. Sugathan, A. Jhingan, B. R. S. Babu, Varughese, K. S. Golda, B. P. Ajith Kumar, B. Sateesh, Santanu Pal, Singh, A. K. Sinha ans S. Kailas, Phys. Rev. C 84, 064606 (2011).

[9] Monika Manhas, Raj K. Gupta, Qingfeng Li, S. K. Patra, and Walter Greiner, Phys. Rev. C **74**, 034603 (2006)

[10] J.Blocki, J.Randrup, W.J. Swatecki and C.F. Tsang, Ann. Phys.(NY) 105, 427(1977)

[11] R. K. Gupta, M. Balasubramaniam, R. Kumar, N.Singh, M.Manhas, and W.Greiner, J. Phys. G: Nucl. Part. Phys. C 31, 631(2005)

[12] J. Maruhn and W. Greiner, Phys. Rev. Lett. 32, 548 (1974)

[13] H. J. Fink, J. Maruhn, W. Scheid and W. Greiner, Z. Phys. 268, 321(1974)

[14] R. K. Gupta, R. K. Gupta and W. Greiner, Phys. Rev. Lett. 35, 353(1975)

[15] R. K. Gupta, M. Balasubramaniam, R. Kumar, N.Singh, M.Manhas, and W.Greiner, J. Phys. G: Nucl. Part. Phys. C 31, 631(2005)

[16] A. Iwamoto, P.Möller, J. R Nix and H.Sagawa, Nucl. Phys. A 596, 329 (1996)

[17] N. Malhotra and R.K. Gupta, Phys. Rev. C 31, 1179 (1985)

[18] T. A. Werke et al. Phys. Rev. C 92, 054617(2015)

[19] J. P. Lestone, Phys. Rev. C 52, 2(1995)

CHAPTER 2:

The Dynamical Cluster-decay Model(DCM)

The Dynamical Cluster-Decay Model [1]-[8] (DCM) is based on Quantum Mechanical Fragmentation Theory, the QMFT [9-11], and is reformulation of the preformed cluster model (PCM) [12-14] ideology which has been exercised to address ground state decays.

DCM is explicitly used to study the decay of excited compound nucleus especially for heavy ion dynamics by including the contributions of the temperature and angular momentum effects along with the deformations and orientations of the decaying fragments. The study of DCM [1]-[9] include various mass regions which on the basis of mass numbers can be categorized as light mass (^{48}Cr*, ^{56}Ni*), intermediate mass (^{116,118,122}Ba*), heavy ($^{176\text{-}196}$Pt*, ^{201}Bi*, ^{202}Pb*, ^{204}Po*, ^{217}Fr*) and super-heavy(Z=105-118).

The DCM works out in terms of the collective coordinates of mass and charge asymmetry $\eta_A=\frac{A_1-A_2}{A_1+A_2}$ and $\eta_Z=\frac{Z_1-Z_2}{Z_1+Z_2}$ and relative separation R where A_1 and A_2 refers to the heavier and lighter fragment respectively. These two coordinates refer, respectively to the nucleon exchange between the fragments after the decay and transfer of kinetic energy of incident channel $E_{c.m}$ to internal excitation (total excitation or total kinetic energy, TXE or TKE) of the outgoing channel, where the CN excitation energy $E_{CN}^{*}=E_{c.m}+Q_{in=}|Qout|+TKE(T)+TXE(T)$ is related to temperature T (in MeV) and is given by:

$$E_{CN}^{*}=\left(\frac{A}{a}\right)T^{2}-T; \tag{1}$$

Where 'a' is level density parameter having range between 9 to 12.

It is to be noted that in the present work, the mass dependent level density parameter [15] has been exercised within the framework of DCM and it reads as:

$$a=\frac{A}{15.54\ MeV}\{1+3.7\times\sqrt[-1]{3}{A}+10.87\times\sqrt[-2]{3}{A}\} \tag{2}$$

In terms of these coordinates, the DCM based cross-sections are estimated by using partial wave analysis as:

$$\sigma=\frac{\pi}{k^{2}}\Sigma_{l}^{l_{max}}(2l+1)P_0P \tag{3}$$

where k is represented by $k=\sqrt{\frac{2\mu E_{c.m.}}{k^{2}}}$ and the reduced mass is given as:

$$\mu=\frac{A_1A_2}{A_1+A_2}m=\frac{1}{4}Am(1-\eta^2) \quad (4)$$

m being the nucleon mass and ℓ_{max} the maximum angular momentum which could be fixed corresponding to the vanishing of the fusion barrier of the incoming channel η_i or the point where 3n cross-sections tends to negligibly small values.

This model is a two-step model

a) First step involves the calculation of quantum mechanical preformation probability P_0 of the decay products or cluster formed in the mother nuclei and refers to the motion in η-coordinates.

b) Second step is the penetration tunnelling of the fragments/ clusters through the Columbic barrier and refers to the motion in R-coordinates.

Both preformation probability and the penetrability depend on ℓ and T of the system, and on deformations $\beta_{\lambda i}$ and orientations θ_i of the two nuclei or fragments. (λ=2, 3, 4, for quadrupole, octupole, hexadecapole deformations).

Preformation Probability, P_0

To calculate Preformation factor (P_0), the stationary Schrödinger wave equation is solved in η-coordinates:

$$\left\{-\frac{\hbar^2}{2\sqrt{B_{\eta\eta}}}\frac{\partial}{\partial\eta}\frac{1}{\sqrt{B_{\eta\eta}}}\frac{\partial}{\partial\eta}+V_R(\eta,T)\right\}\psi^{\nu}(\eta)=E^{\nu}\psi^{\nu}(\eta) \quad (5)$$

with ν = 0,1,2,3,….. referring to ground state (ν = 0) and excited state solutions. The mass parameters $B_{\eta\eta}$, are the smooth classical hydro-dynamical masses [16], which represents the kinetic energy part as the contribution of shell effects at higher temperature is negligible. The mass parameters $B_{\eta\eta}$ is given by:

$$\beta_{\eta\eta}=\frac{AmR^2}{4}\left[\frac{v_t(1+\gamma)}{v_c(1+\delta^2)}-1\right] \quad (6)$$

With

$$\gamma=\frac{R_c}{2R}\left[\frac{1}{1+cosv_1}\left(1-\frac{R_c}{R_1}\right)+\frac{1}{1+cos\,v_2}\left(-\frac{R_c}{R_2}\right)\right] \quad (7)$$

$$\delta = \frac{1}{2R}[(1 - cosv_1)(R_1 - R_C) + (1 - cosv_2)(R_2 - R_c)] \quad (8)$$

The preformation probability is calculated by solving Schrodinger equation (5) and reads as

$$P_0 = |\psi_R^0(A_2)|^2 \frac{2}{A}\sqrt{\beta_{\eta\eta}}(A_2) \quad (9)$$

Fragmentation Potential

The temperature dependent potential used in this Schrodinger equation is given by

$$V_R(\eta, T) = \sum_{i=1}^{2}[V_{LDM}(A_i, Z_i, T)] + \sum_{i=1}^{2}[\delta U_i]\exp(-T^2/T_0^2) + V_c(R, Z_i, \beta_{\lambda i}, \theta_i, T) + V_P(R, A_i, \beta_{\lambda i}, \theta_i, T) + V_\ell(R, A_i, \beta_{\lambda i}, \theta_i, T) \quad (10)$$

where the T-dependent terms Vc, V_P and V_ℓ are defined as follows: Vc is the Coulomb potential, V_P is the proximity potential for hot deformed nuclei and V_ℓ is the potential due to rotational motion of hot deformed nuclei.

Further, in Eq. 12, the macroscopic (LDM) and microscopic (shell corrections) parts are contained, which allow us to define the binding energy B of a nucleus at temperature T is defined as the sum of liquid drop energy V_{LDM} (T) and shell correction δU (T) i.e.

$$B(T) = V_{LDM}(T) + \delta U exp\frac{-T^2}{T_0^2} \quad (11)$$

The T dependent liquid drop part of the binding energy V_{LDM} (T) is calculated from Davidson et al.[17], based on the semi-empirical mass formula of Seeger [18].

$$V_{LDM}(A, Z, T) = \alpha(T)A + \beta(T)A^{\frac{2}{3}} + \left(\gamma(T) - \frac{\eta(T)}{A^{\frac{2}{3}}}\right)\left(\frac{I^2+2|I|}{A}\right) + \frac{Z^2}{R_0(T)A^{\frac{2}{3}}}\left(1 - \frac{0.7636}{Z^{\frac{2}{3}}} - \frac{2.29}{\left[R_0(T)A^{\frac{1}{3}}\right]^2}\right) + \delta(T)\frac{f(Z,A)}{A^{\frac{3}{4}}} \quad (12)$$

As there is no microscopic shell model known for shell corrections of light nuclei, we use the empirical formula of Myers and Swiatecki [12], for the shell correction δU in Eq. 11.

Types of potentials

The remaining three terms in eq. (12) can be explained as follows:

Coulomb potential (V_c)

The Coulomb potential describes the force of repulsion acting between the interacting nuclei/outgoing fragments during a reaction due to charges present on them.

The Coulomb potential for two interacting spherical nuclei is given as: [20, 21]

$$V_c = \frac{Z_1 Z_2 e^2}{R} \quad (13)$$

The Coulomb potential for hot and rotating, deformed and oriented nuclei given as:

$$V_C(Z_i, \beta_{\lambda i}, \theta_i, T) = \frac{Z_1 Z_2 e^2}{R(T)} + 3Z_1 Z_2 e^2 \sum \lambda, i = 1{,}2 \frac{R_i^{\lambda}(d_i, T)}{(2\lambda+1)\mathrm{R(T)}^{\lambda+1}} \quad (14)$$

The Proximity Potential (V_P)

Blocki et al. [22] have reanalysed and extended a theorem, according to which the force between two gently curved surfaces in close proximity is proportional to the interaction potential per unit area between the two flat surfaces. The original expression of Blocki based on the pocket formula was for spherical nuclei, and is given as

$$V_P(s_0) = 4\pi \bar{R} \gamma b \Phi(s_0). \quad (15)$$

$\Phi(s_0)$ is the universal function which is dependent on the minimum separation distance and is independent of the shapes of nuclei or the geometry of nuclear system. Here $\bar{R}$ is the mean curvature radius of the reaction partners, characterizing the gap. γ and b respectively represent the specific nuclear surface as discussed in [23].

The value of b~1fm and the minimum separation distance s_0 is defined in units of b as s_0/b.

Centrifugal Potential (V_ℓ)

The rotational motion gives an additional energy due to the angular momentum defined as [20, 21]

$$V_{\ell}=\frac{\hbar^2 l(l+1)}{2I_S(T)} \quad (16)$$

with $\mu=\frac{A_1A_2}{A_1+A_2}m$ as the reduced mass m is the nucleon mass. In the complete sticking limit, the moment of inertia (I) is given as,

$$I = I_s = \mu R^2 + \frac{2}{5}A_1 m R_1^2 + \frac{2}{5}A_2 m R_2^2$$

and corresponding non-sticking limits of moment of inertia is $I = I_{NS} = \mu R^2$

It is relevant to mention here that value of angular momentum extracted experimentally, is based upon moment of inertia limit.

Penetration Probability P

Penetrability P measures the capability of fragment nucleus to penetrate the potential barrier generalized during compound nucleus formation. The penetrability P is the WKB integral between R_a and R_b.

$$P = exp\left[\frac{-2}{\hbar^2}\int_{R_b}^{R_a}\left\{2\mu[V(R) - Qeff]^{\frac{1}{2}}dR\right\}\right]$$

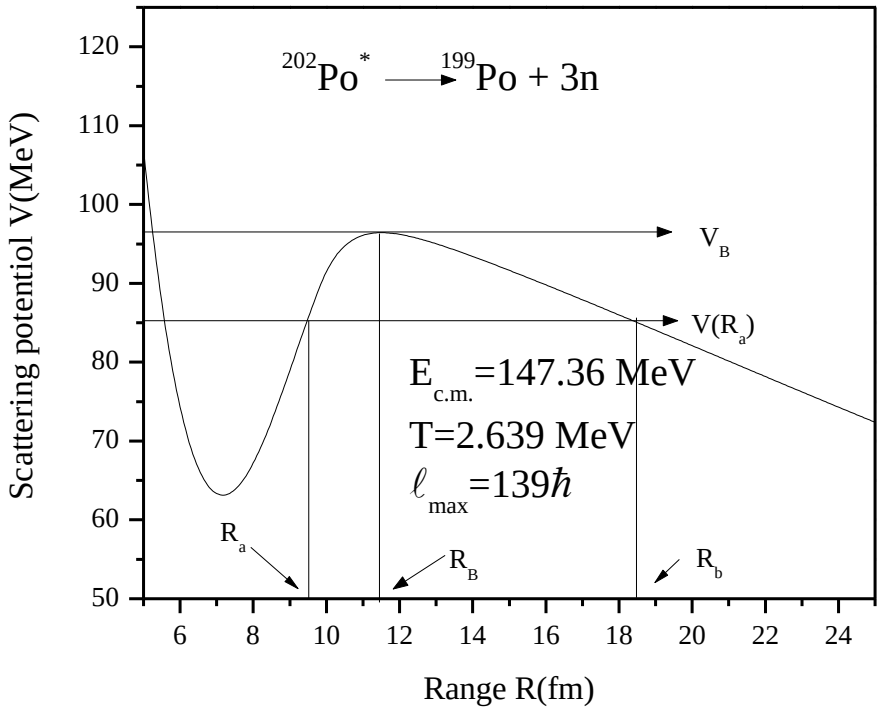

Fig 2.1 Scattering Potential

Here first turning point is given as:

$$R_a = R_t + \Delta R(T)$$

Where $R_t = R_1 + R_2$ (shown in fig. 2.1) and $\Delta R(T)$ is the neck length parameter that assimilates the neck formation effects. R_B represents the barrier height and R_b shows the near saddle location or (exit point) of decaying fragments. The relevant details are depicted in Fig 2.1, where scattering potential is plotted as a function of Range R (fm), for decay of $^{202}Po^{*}$ nucleus into 3n cluster and compliment daughter ^{199}Po.

References:

[1] R. K. Gupta, M. Balasubramaniam, R. Kumar, D. Singh, and C. Beck, Nucl. Phys. A **479-482** (2004); M. Kaur, and M. K. Sharma, Eur. Phys. J. A **50**, 61 (2014).

[2] R. K. Gupta, S. K. Arun, R. Kumar, and M. Bansal, Nucl. Phys. A **834**, 176c-179c (2010).

[3] D. Jain, R. Kumar, M. K. Sharma, and R. K. Gupta, Phys. Rev. C **85**, 024615 (2012).

[4] R. Kumar, K. Sandhu, M. K. Sharma, and Raj K. Gupta, Phys. Rev. C **87**, 054610 (2013); K. Sandhu, G. Kaur and M. K. Sharma, Nucl. Phys. A **921** 114 (2014).

[5]G. Sawhney and M. K. Sharma, Eur. Phys. J. A **48** 57 (2012); G. Kaur and M. K. Sharma, Phys. Rev. C **87** 044601 (2013); G. Kaur, D. Jain, R. Kumar, M. K. Sharma, Nucl. Phys. A **916**, 260(2013).

[6]G. Sawhney, G. Kaur, M. K. Sharma, and R. K. Gupta Phys. Rev. C **88** 034603 (2013).

[7] M. Kaur, R. Kumar, and M. K. Sharma, Phys. Rev. C **85** 014609 (2012); K. Sandhu, M. K. Sharma and R. K. Gupta, Phys. Rev. C **85**, 024604 (2012).

[8] R. K. Gupta, M. Balasubramaniam, R. Kumar, N. Singh, M. Manhas, and W. Greiner, J. Phys. G: Nucl. Part. Phys. **31**, 631 (2005); R. K. Gupta, Monika Manhas, and W. Greiner, Phys. Rev. C **73**, 054307 (2006).

[9] J. Maruhn and W. Greiner, Phys. Rev. Lett. 32, 548 (1974)

[10] H. J. Fink, J. Maruhn, W. Scheid and W. Greiner, Z. Phys. 268, 321(1974)

[11] R. K. Gupta, R. K. Gupta and W. Greiner, Phys. Rev. Lett. 35, 353(1975)

[12] S. S. Malik and R. K. Gupta, Phys. Rev. C 39, 1992(1989)

[13] S. Kumar and R. K. Gupta, Phys. Rev. C 55, 218(1997)

[14] R. K. Gupta, in *Heavy Elements and Related New Phenomena*, edited by W. Greiner and R. K. Gupta (World Scientific, Singapore, 1999), Vol. II, Chap. 18. P. 730

[15] J. P. Lestone, Phys. Rev. C 52, 2(1995)

[16] H. Kröger and W. Scheid, j. Phys. G: Nuel. Part. Phys. 6. L85(1980)

[17] N. J. Davidson, S. S. Hsiao, J. Markram, H.G. Miller, and Y. Tzeng, Nucl. Phys . A 570, 61c(1994)

[18] P. A. Seeger, Nucl. Phys .25, 1(1961) .

[19] W.D. Myers and W.J. Swiatecki, Nucl. Phys . A 81, 1(1966)

[20] R. K. Gupta, in *Clusters in Nuclei*, edited by C.Beck, lecture notes in physics 818(Springer-Verlag, Berlin, Heidelberg, 2010), Vol.1, 223-264.

[21] R. K. Gupta, M. Balasubramaniam, R. Kumar, N. Singh, M. Manhas, W. Greiner, J. Phys. G: Nucl. Part. Phys. 31, 631(2005)

[22] J. Blocki, J. Randrup, W. J. Swiatecki, and C. F. Tsang, Ann. Phys. (NY) 105, 427(1977)

[23] R. K. Gupta, M. Balasubramaniam, R. Kumar, N.Singh, M.Manhas, and W.Greiner, J. Phys. G: Nucl. Part. Phys. C 31, 631(2005)

Chapter-3

Results and Discussions

The present work deals with the analysis of decay of compound nucleus formed in ^{44}Ca-induced reactions with actinide targets. The cross-sections for the decay of compound nucleus ^{202}Po*, ^{203}At* and ^{206}Rn*formed in reactions ^{44}Ca+^{158}Gd, ^{44}Ca+^{159}Tb and ^{44}Ca+^{162}Dy via neutron evaporation are addressed within the framework of DCM. Initially, the calculations are done by taking level density parameter a=9 but the data could not be addressed successfully. To account for this, the constant values of level density parameter are replaced with mass- dependent level density parameter in ref to [1]. In earlier works [2], the use of mass dependent level density parameter was found to be adequate to address neutron evaporation data for compound nucleus with mass A≥ 200. In view of this, the use of mass dependent level density parameter also proves to be useful for the address of data. The decay of compound systems ^{202}Po*, ^{203}At* and ^{206}Rn* formed in reactions ^{44}Ca+^{158}Gd, ^{44}Ca+^{159}Tb and ^{44}Ca+^{162}Dy is investigated using DCM[3-7] and the decay patterns are analyzed in view of fragmentation potential and preformation factor.

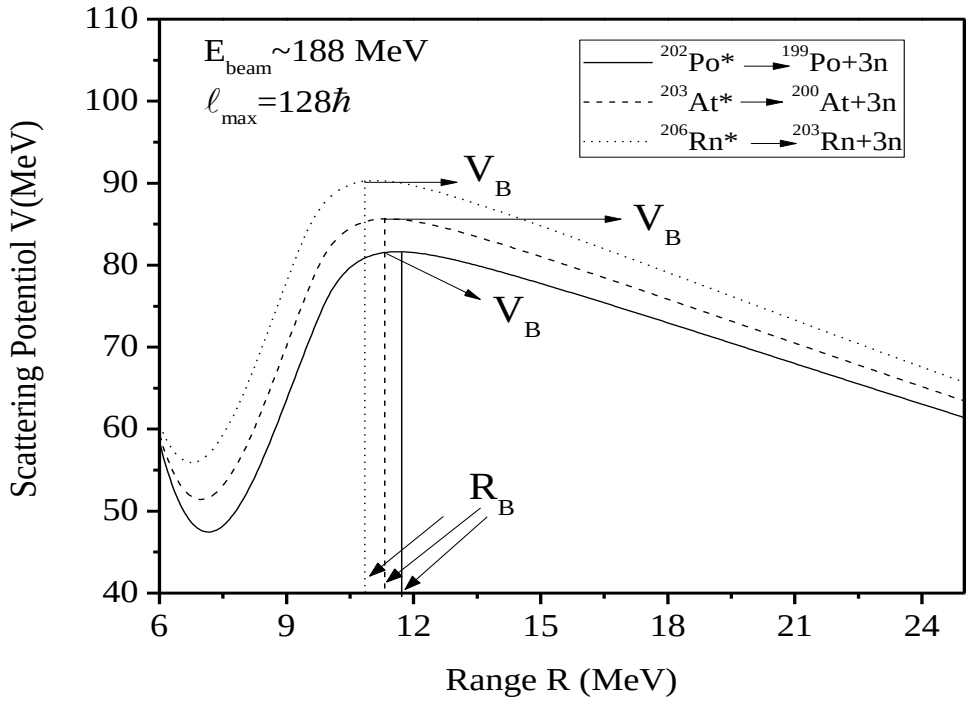

Fig 3.1 Scattering potential plotted as a function of range R(fm) for ^{202}Po *, ^{203}At* and ^{206} Rn* at common beam incident energy.

First of all, the scattering potential of the three compound systems ^{202}Po *, ^{203}At* and ^{206} Rn* is plotted as a function of Range R (fm) at common incident beam energy E_{beam}= 188 MeV and ℓ_{max}=128$\hbar$ as shown in Fig 3.1 to study the tunnelling of decaying fragments across the

barrier. From above figure, it is clear that with rise in the mass of the decaying system, the barrier height V_B increases and becomes maximum for ^{206} Rn* . A noticable change can also be seen in the position of the barrier R_B and it is observed that the barrier position shifts towards lower range R with increase in mass of compound system.

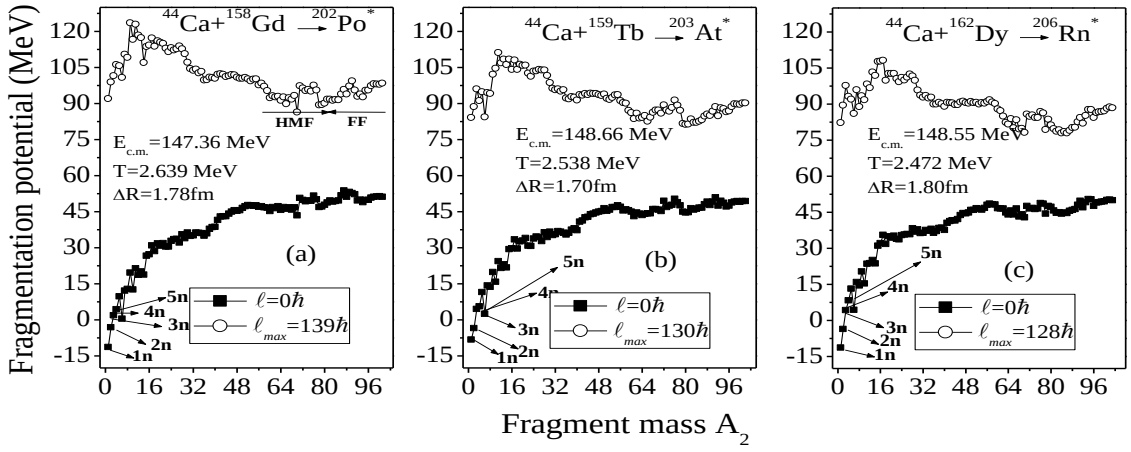

Fig 3.2 Variation of fragmentation potential, V_η with fragment mass, A_2 for the decay of (a)^{202}Po*, (b) ^{203}At* and (c) ^{206}Rn* at common incident beam energy E_{beam}~188 MeV plotted at ℓ=0$\hbar$ and ℓ=ℓ_{max}

In Fig 3.2, the fragmentation potential is plotted as function of fragment mass A_2, for the decay of compound nucleus ^{202} Po*, ^{203}At* and ^{206}Rn* at common incident beam energy E_{lab}= 188 MeV corresponding to respective centre of mass energy E_{cm}=147.36, 148.66 and 148.55 MeV at corresponding best fit values of neck length parameter. The filled squares represented in fig 3.2, show the fragmentation potential at angular momentum ℓ=0ħ, whereas the hollow spheres represent the values for corresponding ℓ_{max} values. In fig 3.2(a), it can be seen that at lower values of angular momentum i.e. ℓ=0ħ, the neutron evaporation i.e. 1n-5n are the dominant decay modes, for the decay of compound nucleus ^{202} Po* as they tend to have lower values of fragmentation potential. Consequently, the possibility of other decay modes i.e. HMF or fission seems to be negligible. On the other hand, when we shift towards the higher angular momentum values i.e. ℓ_{max}=139ħ, the plot shows small valley in the region A_2= 60-100, where the region A_2=60-80 signifies HMF and the region with A_2≅80-100 signifies fission fragments. This means for higher angular momentum values, i.e. ℓ=ℓ_{max}, the neutron evaporation from the compound nucleus ^{202} Po* is also accompanied by some heavy mass fragments (HMF's) and fission fragments. Thus we can say that the compound nucleus ^{202}Po* prefers to decay via neutron evaporation at low angular momentum values, while there

is a possibility of competing fission like decay channel at higher ℓ values. Similar results were observed for the decay of compound nucleus $^{203}At^{*}$ and $^{206}Rn^{*}$ as shown in Fig 3.2(b) and 3.2(c). These two compound systems also tend to decay via neutron evaporation at lower angular momentum values while at higher angular momentum values, a few HMF's and fission fragments also start competing in the decay path. The best fit values of ΔR for these systems are ΔR= 1.78fm, 1.70fm and 1.80fm and corresponding ℓ_{max} values are139ħ, 130ħ and 128ħ.

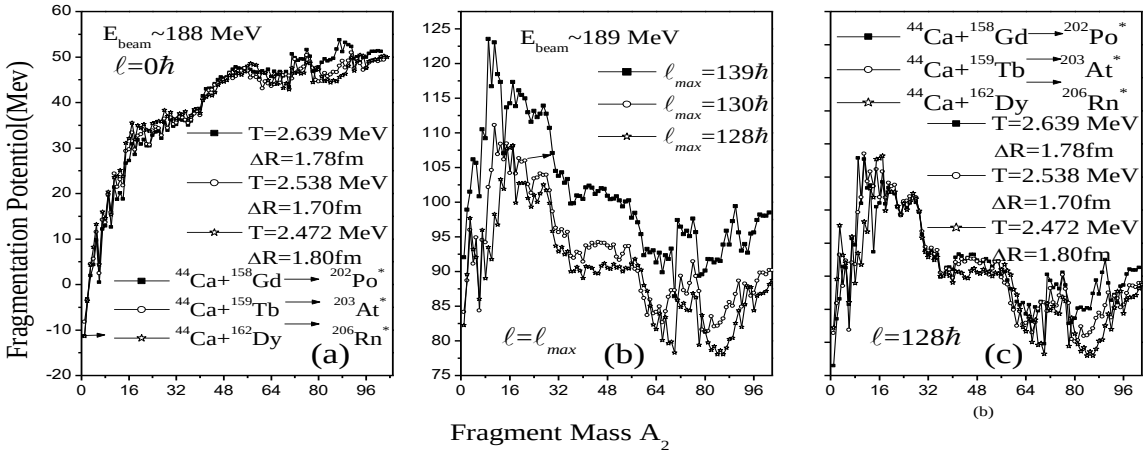

Fig 3.3 Variation of fragmentation potential, Vη with fragment mass, A_2 for the decay of $^{202}Po^{*}$, $^{203}At^{*}$ and $^{206}Rn^{*}$ at common incident beam energy E_{beam}~188MeV at (a) ℓ=0ħ, (b)$\ell=\ell_{max}$ and (c)ℓ=128ħ

Further to do a comparative analysis of the fragmentation structure of the decay of all the three compound nuclear systems, the fragmentation potential for all the three systems, Po*, At* and Rn* is plotted as a function of fragment mass A_2 at common beam energy E_{beam}=188 MeV as shown in Fig 3.3. It is noted that the graph is plotted at the respective best fit values of ΔR and corresponding values of temperature are shown. In Fig 3.3 (a), the fragmentation potential is plotted at ℓ=0ħ and it is clear from the figure that all the three compound nuclei undergo similar kind of fragmentation behaviour as they consistently show clear preference for neutron evaporation path. Only small variations in magnitude are observed and fission region seems completely absent. In addition to this, the fragmentation structures are also compared at higher ℓ –values. For this, the fragmentation potential is plotted as a function of fragment mass A_2 but for ℓ_{max} values as shown in Fig 3.3(b) and at common higher angular momentum values ℓ=128ħ. From Fig 3(b), again it is inferred that the decay profile of all

these systems is almost identical at higher angular momentum values, with some change in the magnitude. Amongst all the three compound systems, ^{206}Rn* has the lowest magnitude of fragmentation potential which signifies that it has relatively higher probability towards decay, provided the beam energy is kept same. Also, if the fragmentation structure is studied at same higher ℓ-values i.e. at ℓ=128$\hbar$ similar and overlapping structures are obtained showing some minor changes in magnitude, which are negligible for light and IMF region but noticeable for HMF and fission region.

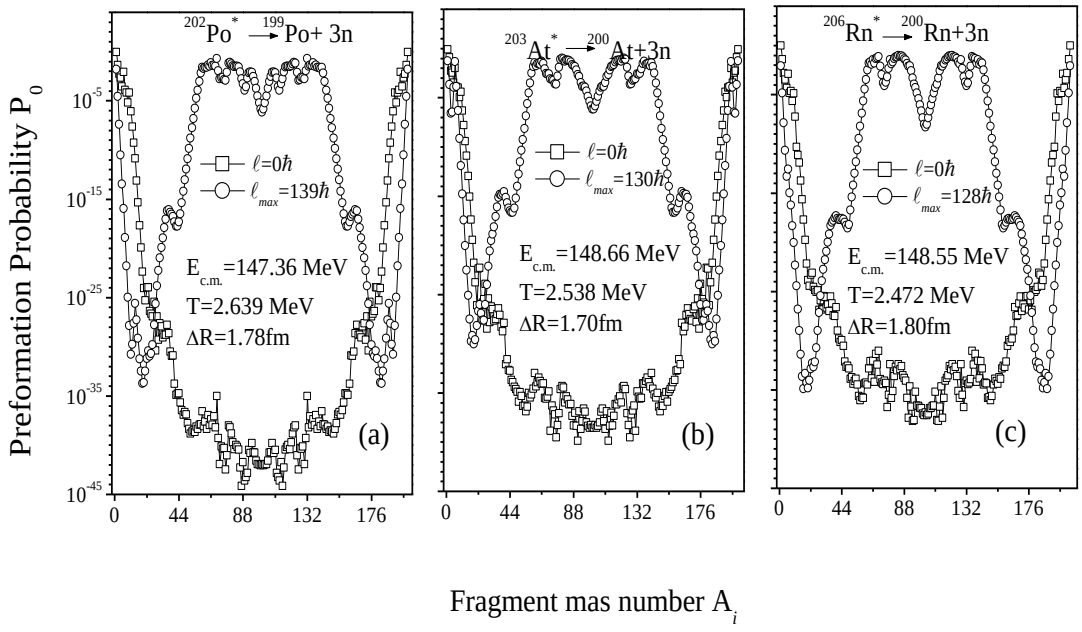

Fig 3.4 Variation of preformation probability, P_0 with fragment mass, A_2 for the decay of (a)^{202}Po*, (b) ^{203}At* and (c) ^{206}Rn* at common incident beam energy E_{beam}~188 MeV plotted at ℓ=0$\hbar$ and ℓ=ℓmax

Further, the decay profiles of the compound systems are analysed from preformation probability P_0 curves as shown in Fig 3.4. Here the preformation probability is plotted as a function of fragment mass number A_i for the decay of three compound systems ^{202}Po*, ^{203}At* and ^{206}Rn* at the common incident beam energy E_{beam}=188 MeV at their respective best fit values of ΔR. Note that the curves are plotted at ℓ=0$\hbar$ and ℓ=ℓ_{max} values for all the three systems. The preformation curves reconfirms the results concluded from the fragmentation potential curve that the compound systems prefer to decay via neutron evaporation at lower ℓ-values, as they have higher P_0 values. As we transmute towards higher angular momentum values, peaks in HMF and fission fragments also start emerging in the decay profiles of all

the three compound systems signifying that HMF and fission fragments also start appearing in the decay of compound nucleus. The Preformation pattern for the three compound systems seems to be asymmetric although the structure is not smooth and a multiple asymmetric sub-peaks can be seen for all the systems.

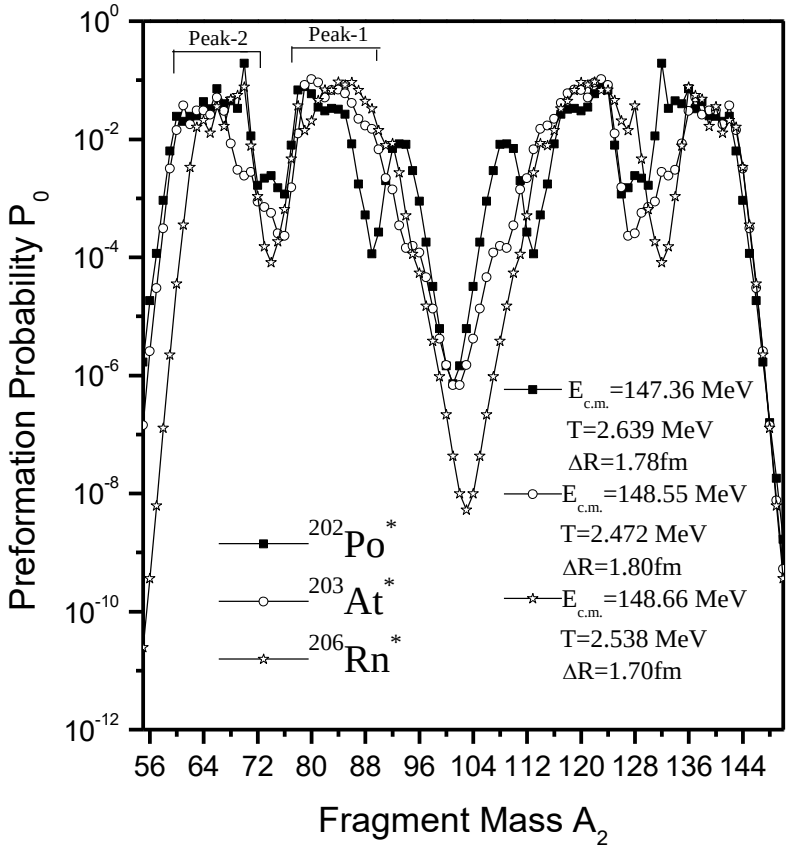

Fig 3.5 Variation of preformation probability, P_0 with fragment mass, A_2 at energy E_{beam}~189 MeV for reactions $^{202}Po^*$, $^{203}At^*$ and $^{206}Rn^*$ at $\ell=\ell_{max}$.

To have a closer look on the asymmetric structure of the decay profile for all the three systems, the preformation probability curve is plotted for A_2= 50-150 at common beam energy and their respective ℓ_{max} values. The corresponding values of $E_{c.m.}$, T and ΔR are also shown in fig 3.5. The figure clarifies that the highest asymmetry in fragmentation is found for the heaviest systems $^{206}Rn^*$ while the fragmentation for $^{202}Po^*$ and $^{203}At^*$ is relatively less asymmetric. Also it is clear that the asymmetric peaks are not smooth in structure and a few secondary peaks corresponding to A_2= 56-96 are also seen.

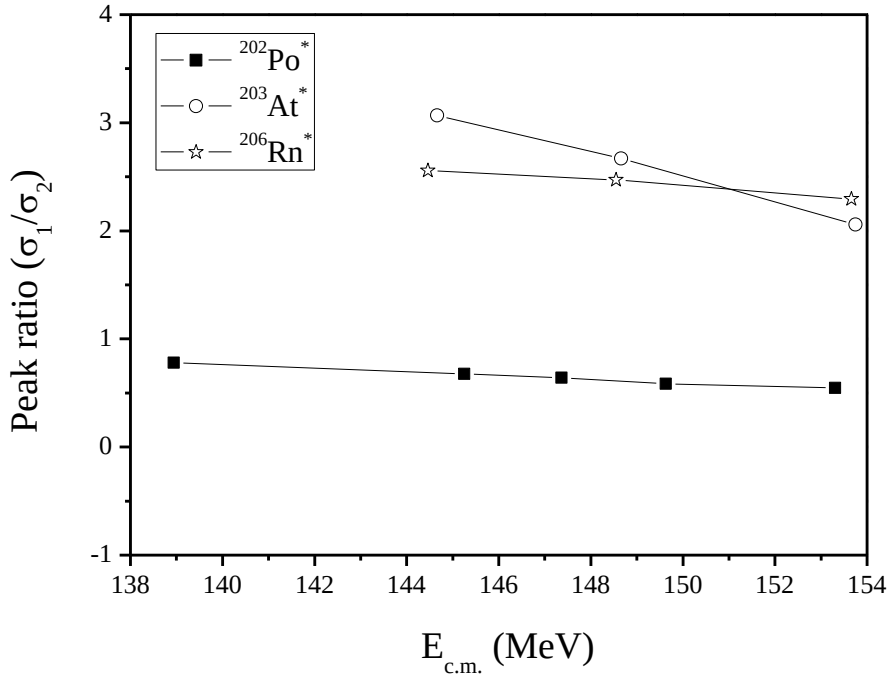

Fig 3.6 Peak Ratios calculated at different centre of mass energies

The peak ratios for the peaks originating in the preformation pattern (shown in Fig 3.5) for all the compound systems are calculated to see their relative contribution towards cross-sections. The peak ratios are plotted as a function of $E_{c.m,}$, as shown in Fig 3.6 and it has been observed that the peak ratios for the lightest mass system i.e. $^{202}Po^{*}$ lies below 1 which means the contribution due to symmetric peak is lesser as compared to asymmetric peak while the trend seems to be reverted for heavier systems where the contribution due to symmetric peaks is higher than that of asymmetric component. At common incident beam energy E_{beam}~188 MeV, the peak ratios for the systems $^{202}Po^{*}$, $^{203}At^{*}$ and $^{206}Rn^{*}$ are 0.64, 2.67 and 2.74 respectively.

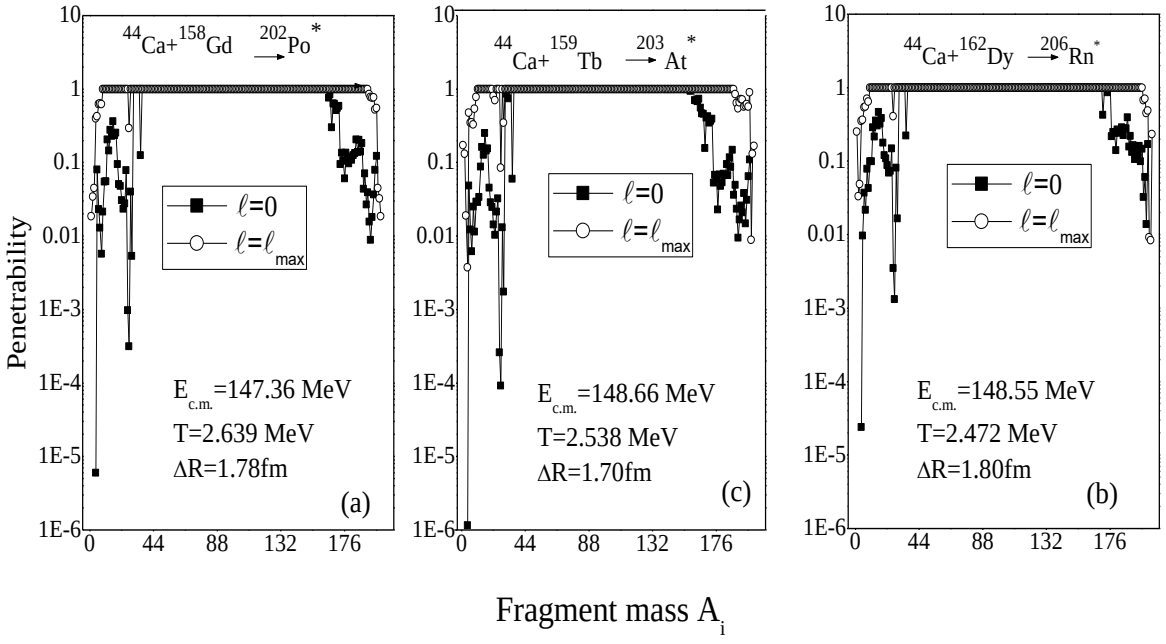

Fig 3.7 Penetrability plotted as a function of fragment mass at different excitation energies for reactions ^{202}Po*, ^{203}At* and ^{206}Rn*

The DCM methodology follows the collective clusterization, which suggests that a particular fragment is preborn within the compound nucleus prior to its decay from the compound system. The preformed fragment then penetrates through the potential barrier comprising of V_C, V_N and V_ℓ. This motivates us to study the penetration probability P of each possible fragment of the given compound systems. In Fig 3.7, penetration probability P calculated via equation, is plotted as a function of fragment mass number A_i at common incident beam energy E_{beam}~188 MeV (corresponding $E_{c.m.}$ =147.36 MeV, 148.55 MeV and 148.66 MeV) for (a) ^{202}Po*, (b) ^{203}At* and (c) ^{206}Rn* respectively at the best fit values of ΔR. Here, the filled squares represent $\ell=0\hbar$ case while the hollow circle represent the penetrability behaviour for $\ell=\ell_{max}$. From the Fig 3.7(a), it is clear that the penetrability curve shows a smooth variation for all the fragments except a few light fragments (and their complementary fragments), and its value lies close to 1. At lower ℓ-values i.e. for $\ell=0\hbar$, the magnitude of penetrability P is relatively small as compared to that at ℓ_{max} which may be attributed to the reason that at lower angular momentum values, the fragments don't possess sufficient

energies to cross through the barrier. Similar behaviour can be seen for $^{206}Rn^{*}$ and $^{203}At^{*}$ in Fig 3.7(b) and 6(c) apart from some variation in magnitude and structure

Table 3.1 DCM based cross-sections compared with experimental data at different excitation energies E^{*}_{CN} for reaction $^{44}Ca+^{158}Gd \longrightarrow ^{202}Po^{*}$

E^{*}_{CN} (MeV)	T (MeV)	ΔR (fm)			ℓmax (ħ)			σ_{DCM} (mb)			σ_{EXPT} (mb)		
		3n	4n	5n	3n	4n	5n	3n	4n	5n	3n	4n	5n
44.552	2.425	1.95	2.7	-	133	114	-	2450	701	-	$2290^{\pm 590}$	$600^{\pm 120}$	-
49.7153	2.558	1.75	2.8	2.8	137	113	112	734	896	112	$910^{\pm 340}$	$1620^{\pm 150}$	$200^{\pm 60}$
50.8885	2.5873	1.83	2.8	2.8	135	112	112	1210	773	112	$1840^{\pm 620}$	$2100^{\pm 230}$	$600^{\pm 130}$
53.0001	2.639	1.78	2.8	2.8	139	115	125	1220	1290	499	$1440^{\pm 440}$	$1940^{\pm 190}$	$620^{\pm 100}$
55.2687	2.694	1.75	2.5	2.8	141	123	116	1250	1260	179	$1020^{\pm 360}$	$1380^{\pm 140}$	$1090^{\pm 120}$
58.942	2.780	1.7	2.3	2.8	142	126	118	755	604	199	$770^{\pm 320}$	$660^{\pm 110}$	$2700^{\pm 180}$

Table 3.2 DCM based cross-sections compared with experimental data at different excitation energies, E^{*}_{CN} for reaction $^{44}Ca+^{159}Tb \longrightarrow ^{203}At^{*}$

E^{*}_{CN} (MeV)	T (MeV)	ΔR (fm)			ℓmax (ħ)			σ_{DCM} (mb)			σ_{EXPT} (mb)		
		3n	4n	5n	3n	4n	5n	3n	4n	5n	3n	4n	5n
44.9961	2.435	1.75	2.4	-	128	117	-	119	150	-	$140^{\pm 20}$	$130^{\pm 20}$	-
48.9971	2.538	1,7	2.46	1.8	130	119	130	89.4	239	23.8	$90^{\pm 25}$	$230^{\pm 20}$	$18^{\pm 8}$
54.0881	2.664	1.6	2.22	1.8	133	126	133	28.8	120	30.2	$23^{\pm 11}$	$120^{\pm 10}$	$34^{\pm 7}$
57.3771	2.742	-	2.0	1.9	-	131	134	-	47.2	54.5	-	$41^{\pm 8}$	$48^{\pm 11}$
63.2461	2.875	-	-	1.8	-	-	139	-	-	34.5	-	-	$33^{\pm 9}$

Table 3.3 DCM based cross-sections compared with experimental data at different excitation energies, E^{*}_{CN} for reaction $^{44}Ca+^{162}Dy \longrightarrow ^{206}Rn^{*}$

E^*_{CN} (MeV)	T (MeV)	ΔR (fm)			ℓmax (ħ)			σ_{DCM} (mb)			σ_{EXPT} (mb)		
		3n	4n	5n	3n	4n	5n	3n	4n	5n	3n	4n	5n
42.4492	2.364	1.82	2.6	-	125	107	-	59.1	52.9	-	$71^{\pm 17}$	$50^{\pm 13}$	-
46.5412	2.472	1.8	2.95	-	128	103	-	69.0	146	-	$59^{\pm 19}$	$130^{\pm 20}$	-
51.6532	2.601	1.7	2.5	2.1	129	114	121	31.8	80.7	22.2	$31^{\pm 11}$	$76^{\pm 14}$	$24^{\pm 7}$
54.8772	2.679	-	2.2	2.0	-	121	125	-	46.3	19.6	-	$55^{\pm 12}$	$20^{\pm 7}$
60.8542	2.818	-	2.0	2.0	-	127-	128	-	17.8	23.6	-	$14^{\pm 7}$	$27^{\pm 7}$

The neutron evaporation cross-sections are calculated within DCM using the product of preformation probability P_0 and penetration probability P by using partial wave analysis (as eq 3 in section-2) by optimising the neck-length parameter ΔR of the model. The calculated cross-sections for 3n, 4n and 5n emission find nice agreement with the experimental data for all the three compound systems except for a few energy points for $^{202}Po^*$. The calculated cross-sections are shown along with the experimental data and other parameters involved in DCM methodology in table 1, 2 and 3 for $^{202}Po^*$, $^{203}At^*$ and $^{206}Rn^*$ respectively.

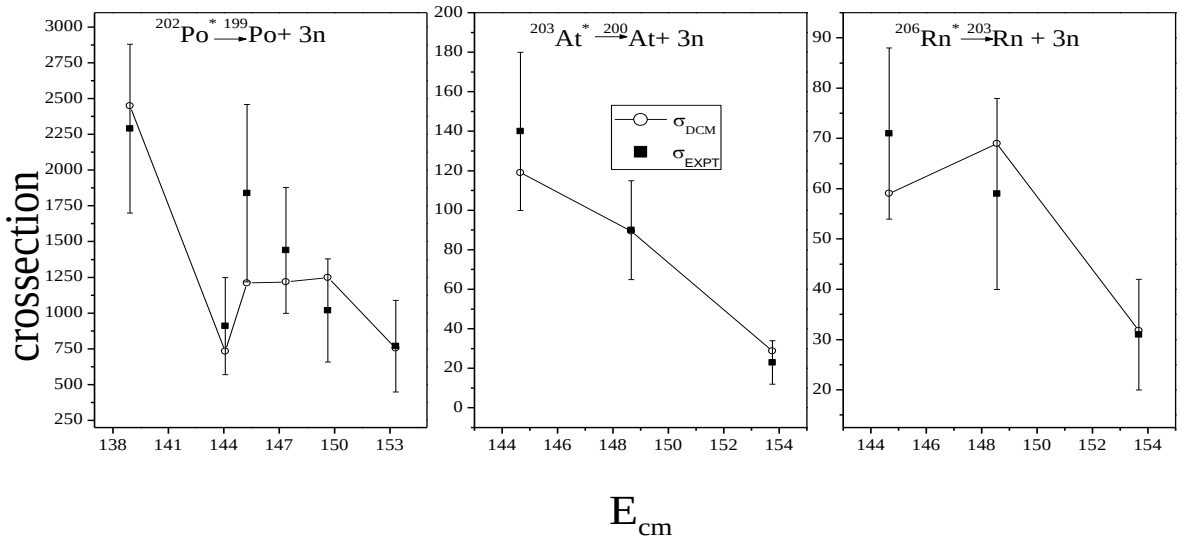

Fig 3.8 DCM based cross-sections and experimental data for composite systems $^{202}Po^*$, $^{203}At^*$ and $^{206}Rn^*$.

Also the comparison for the DCM calculated cross-sections for 3n-emission for all the three systems $^{202}Po^*$, $^{203}At^*$ and $^{206}Rn^*$ can be seen from Fig 3.8 where the cross-sections σ_{DCM} are plotted as a function of $E_{c.m.}$ over the energy range explored in experiment[8]. The

experimentally available cross-sections are also plotted in the curve (filled circles) along with the error limit.

References:

[1] J. P. Lestone, Phys. Rev. C 52, 2(1995)

[2] A. Kaur, K. Sandhu and M. K. Sharma, AIP conference proceedings 1728, 020424(2016)

[3] D. Jain, R. Kumar, M. K. Sharma, and R. K. Gupta, Phys. Rev. C **85**, 024615 (2012).

[4] R. Kumar, K. Sandhu, M. K. Sharma, and Raj K. Gupta, Phys. Rev. C **87**, 054610 (2013); K. Sandhu, G. Kaur and M. K. Sharma, Nucl. Phys. A **921** 114 (2014).

[5]G. Sawhney and M. K. Sharma, Eur. Phys. J. A **48** 57 (2012); G. Kaur and M. K. Sharma, Phys. Rev. C **87** 044601 (2013); G. Kaur, D. Jain, R. Kumar, M. K. Sharma, Nucl. Phys. A **916**, 260(2013).

[6]G. Sawhney, G. Kaur, M. K. Sharma, and R. K. Gupta Phys. Rev. C **88** 034603 (2013).

[7] M. Kaur, R. Kumar, and M. K. Sharma, Phys. Rev. C **85** 014609 (2012); K. Sandhu, M. K. Sharma and R. K. Gupta, Phys. Rev. C **85**, 024604 (2012).

[8] T. A. Werke et al. Phys. Rev. C 92, 054617(2015)

Summary:

The present work deals with the investigation of ^{44}Ca- induced dynamics by studying the related decay patterns of compound nuclei ^{202}Po*, ^{203}At* and ^{206}Rn* formed in the reactions ^{44}Ca+^{158}Gd, ^{44}Ca+^{159}Tb and ^{44}Ca+^{162}Dy within the framework of DCM. The calculations are done by using quadrupole deformations (β2- deformations) for hot- fragmentation and by the use of mass-dependent level-density parameter within the context of DCM-based calculations. The cross-sections for the neutron-evaporation i.e. 3n, 4n and 5n emission from the compound nuclei are addressed by varying the neck-length parameter ΔR of the model and the experimental data finds nice agreement with the DCM based cross-sections. The study of scattering potential for 3n evaporation from the compound systems ^{202}Po*, ^{203}At* and ^{206}Rn* shows that a shifting in barrier height V_B and barrier position R_B is observed as the mass of the compound system formed in ^{44}Ca induced reactions gets enhanced. The barrier height V_B increases with increase in mass while the barrier position R_B shifts to lower range values. The comparative analysis of the fragmentation potential and preformation probability curves has been done and the following points have been observed (i) the considered compound nuclei ^{202}Po*, ^{203}At* and ^{206}Rn* decay via neutron evaporation at lower angular momentum values while as we move towards higher angular momentum values, certain fragments in the heavy mass region also start appearing in the decay channel. (ii) All the three compound systems undergo almost identical fragmentation profile with some variations in structure and magnitude only in light as well as IMF region. (iii) The analysis of preformation probability shows that all the three systems undergo double humped fission structure where fragments A_2=56-96 contribute the most in the decay pattern. (iv)The double humped pattern is broadly categorised in the form of symmetric and asymmetric peaks referred as peak 1 and peak 2. (v) To explore sub structure effect within fission fragments, the peak ratio is evaluated. In addition to this, penetration probability of the fragment decaying through the potential barrier is also studied as a function of fragment mass and it reveals that the light particles (plus complementary fragments) have lesser penetration probabilities as compared to heavier fragments. The DCM based cross-sections seem to show good agreement with experimental data and are tabulated in tables 3.1-3.3 along with other parameters of DCM.